Journal of Electronic Materials, Vol. 23, No. 10, 1994

Coarsening of Three-Dimensional Droplets by Two-Dimensional Diffusion: Part I. Experiment

J.R. ROGERS

National Research Council, Space Science Laboratory, NASA Marshall Space Flight Center, Huntsville, AL 35812

J.P. DOWNEY, W.K. WITHEROW, B.R. FACEMIRE, and D.O. FRAZIER

Space Science Laboratory, NASA Marshall Space Flight Center, Huntsville, AL 35812

V.E. FRADKOV, S.S. MANI, and M.E. GLICKSMAN

Rensselaer Polytechnic Institute, Troy, NY 12180-3590

An experimental study of diffusional coarsening, or Ostwald ripening, in a liquid-liquid two-phase system is described. An experiment performed at its isopycnic point, 42°C, allowed observations for the long times required to investigate coarsening. A holographic technique was instrumental in this work. Holograms taken *in situ* permit investigation of details regarding both the influence of local environmental conditions on individual droplet size histories and measurement of global averages. This study utilized a 100 μm pathlength test cell. The discrete phase was nucleated on one wall of the cell. This configuration resembles island formation in thin film growth. Observation of Ostwald ripening over a period of 1×10^7 s (~4 mo.) reveals that droplet number decays as $t^{-0.733}$ and the average radius increases as $t^{0.247}$, in the asymptotic limit. This shows good agreement with theoretical predictions for diffusional growth of spherical caps on a two-dimensional substrate which is a valid approximation for the geometry of this experiment. Part I of this paper describes the experimental results. Part II discusses a numerical model for droplet growth in a comparison with the experimental results.

Key words: Diffusion, holography, kinetics, microstructure coarsening, Ostwald ripening, phase transformation

INTRODUCTION

Ostwald ripening is the process by which larger droplets grow at the expense of smaller ones, by diffusion of mass away from droplets below a critical radius toward ones above this critical size. The phenomenon is important in many disciplines. Of particular interest to materials processing is its influence on the time dependence of droplet (or particle) size distributions of a precipitated phase.

The objective of this work was to perform an experimental study of the development of microstructures and the growth of a second phase in a two-phase system. To a large extent, growth and distribution of the discrete phase determine the mechanical and electronic properties of an alloy. A detailed understanding of microstructure is essential to predicting the behavior of a material. For example, the formation and growth of clusters in semiconductor thin film deposition result in microstructures which dictate film properties in a device application. Most modeling and experimental studies focus on the average particle and the late stages of growth processes. However, the behavior of the "weakest link" rather than an average property is fundamental to developing predictability regarding practical problems such as fracture analysis in metal fatigue. The unique capabilities provided by holographic tech-

(Received March 1, 1994; revised June 8, 1994)

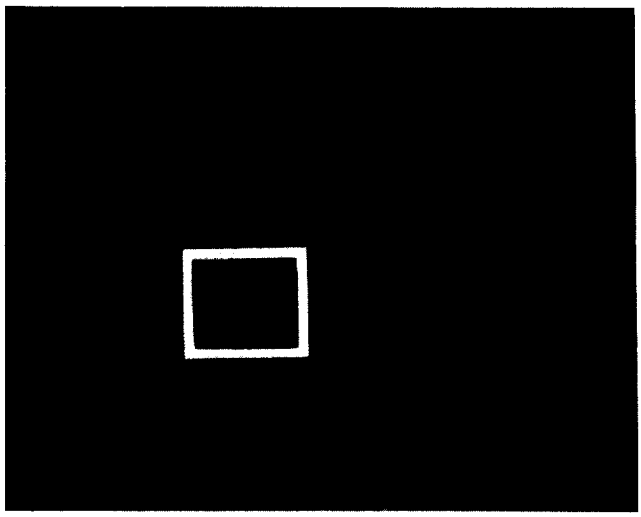

Fig. 1. Projected image of the test cell. The white box indicates the area selected for analysis.

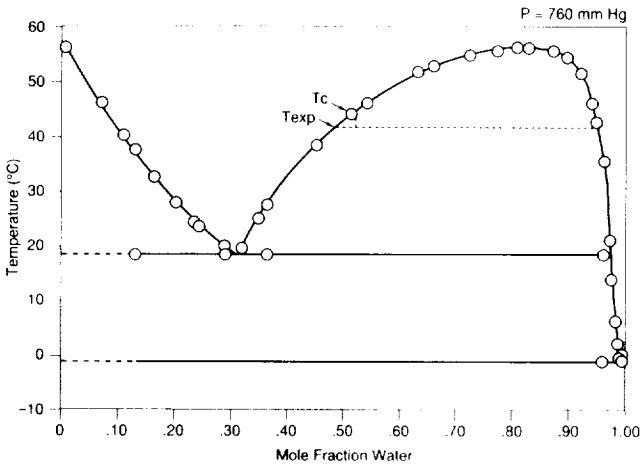

Fig. 2. Succinonitrile/water phase diagram; T_c and T_{exp} represent the consolute and experiment temperatures, respectively.

niques allow detailed analyses of both local dynamic behavior within the context of a particle ensemble and resulting microstructures from a statistically significant population.

The theoretical analysis of coarsening of the droplets requires solving the moving boundary diffusion problem (Stefan problem) with boundary conditions at the test cell walls and at the surfaces of the droplets. The boundary condition imposed on the droplet surfaces is given by the linear form of the Gibbs-Thompson equilibrium equation

$$c(R) = c_0 \cdot \left(1 + \frac{L}{R}\right), \qquad (1)$$

where c(R) is the equilibrium concentration at the surface of the droplet with radius R, c_0 is the equilibrium concentration at the plane interface, and L is the Gibbs-Thompson characteristic length, given by

$$L = \frac{2\gamma\Omega}{kT}, \qquad (2)$$

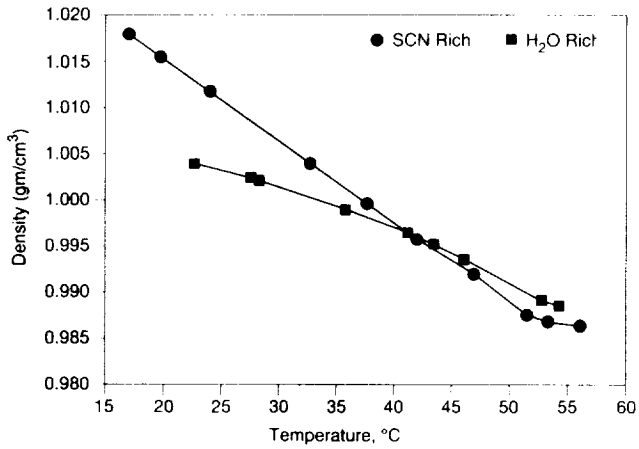

Fig. 3. Densities of equilibrium phases in succinonitrile/water as functions of temperature.

where γ is the interfacial tension, Ω is the molecular volume, k is the Boltzmann constant, and T is the temperature.

In their classical studies of the ripening process Lifshitz, Slyozov, and Wagner (LSW)[1,2] and Todes[3] applied the steady state approximations to the diffusion process. This approximation is valid for the case of very low supersaturation where the characteristic diffusion time is much less than the time required for a significant change in the droplet radius. Using this approach, they determined global scaling laws for the case of three-dimensional diffusion processes. The length scale for the ripening process can be considered to be the average droplet size which predictably grows as $t^{1/3}$ for the latter stages of a three-dimensional diffusional growth. The decrease in the number of droplets as a function of time for the three dimensional case is given by $N(t) \propto t^{-1}$.[1,2] Experimental investigations and numerical simulations support this scaling prediction.

Ripening processes follow different scaling laws in a two-dimensional system. An example of this is the growth of spherical caps on a two-dimensional substrate. Theoretical arguments by Chakraverty for multiparticle diffusion between three-dimensional particles with mass transport restricted to two-dimensions predict $N(t) \propto t^{-3/4}$ and that length scales as $t^{1/4}$.[4] Slyozov obtained the same result for interacting three-dimensional clusters located on a planar substrate.[5] Both Chakraverty and Slyozov utilized the mean-field approximation for their two-dimensional concentration field and assumed implicitly a low volume fraction of droplets. Their prediction has been observed experimentally.[6] Part II of this paper describes the development of a numerical model of three-dimensional droplet growth due to two-dimensional diffusion.

This study employed holography to record the ripening processes in the experimental test cell. The holograms, permanent records of the wavefront, may be reconstructed and the wavefront precisely reproduced. The reconstructed wavefront gives an exact three-dimensional reproduction of the test cell con-

tents at the instant of exposure. Each hologram allows measurement of all the droplet radii in the test cell at a given instant of time. During reconstruction, the hologram image can be moved with relative ease, and the entire test cell volume can be investigated by stepping the field-of-view through a magnified reconstructed image of the test cell. A square region consisting of 25 fields of view (about 5% of the recorded test cell volume), initially populated with 187 droplets, comprised the area selected for analysis. Figure 1 shows a projection of the test cell indicating the area chosen for detailed analysis. It is important to note that the holographic records archive a great deal of additional data.

MATERIALS AND METHODS

All theoretical models of the Ostwald ripening consider growth only due to diffusion. A test of this theory required an experiment devised to study nearly pure diffusional growth by simultaneously eliminating coalescence and convection. Solutions of succinonitrile/water (SCN/H_2O) offer an experimentally convenient model system for the study. Figure 2 shows the phase diagram for SCN/H_2O.[7] Above the critical consolute temperature, 56°C, SCN/H_2O forms a single phase.

When compositions spanning the miscibility gap of the phase diagram are cooled through the coexistence curve, the system separates into droplets of one liquid dispersed in another. Unlike metallic alloys, both the droplet and surrounding phases are transparent, and the growth of the former may be followed by optical means in situ. Moreover, because the phase separation occurs near room temperature, elaborate furnaces for temperature control are not required as would be the case for metals. These experiments were performed near the isopycnic temperature of approximately 42°C (Fig. 3). The droplets were located on the inside wall of a 100 μm pathlength optical cell. During the observation period which spanned about four months, the droplet positions remained unchanged.

The SCN/H_2O system is well characterized as a transparent model for observations of metallic monotectic solidification phenomena[8] and, therefore, was the system of choice for the Ostwald ripening studies. Succinonitrile was vacuum-distilled twice at a measured pressure of 10–20 mm Hg. Water was distilled and filtered through a Millipore Milli-Q water system giving a resistivity of 18 Mohm cm. Approximately equal volumes of the two components were mixed in a waterjacketed separatory funnel and allowed to equilibrate at about 45°C. Aliquots of the water-rich phase extracted from this solution, when cooled at 42°C, resulted in SCN-rich droplets. This phase was selected to assure that the nucleating phase would not wet and spread on the quartz test cell walls. Figure 4 shows nonwetting SCN-rich droplets on a quartz plate.

Experiment Test Cell and Apparatus

A commercially available micro cylindrical spectrophotometer cell shown in Fig. 5 having an optical path length of 100 μm yielded particle densities low enough to allow holographic imaging with good resolution.[9] A 6 in. length of glass tubing attached to the cell fill port permitted sealing. Filling the cell consisted of extracting the lower phase from the reservoir thermostated at 45°C in a heated pipette, wiping the pipette to remove excess upper phase, and expelling the solution into the cell, while maintaining homogeneity by gently heating the pipette with a hot air gun. After the filling operation, the glass extension tube was sealed. Submerging the cell body in an ice bath prevented the solution from significantly changing composition due to vaporization during the sealing procedure. Heating the cell to 46°C for 48 h prior to the experiment assured solution homogeneity. The cell was transferred to the isothermal test chamber held at 46.4°C. Scattering of the laser light during a slow quench determined the actual consolute point to be 45.01°C. After reheating to 46.3°C for 24 h, stepwise quenching into the miscibility gap initiated the experiment. Observations taken during the quench assured the low volume fraction of discrete phase required for optical resolution considerations and for comparison to theory. A test chamber temperature of 42.5°C, close to the neutral buoyancy temperature, yielded an

Fig. 4. Photograph of succinonitrile-rich droplet on quartz.

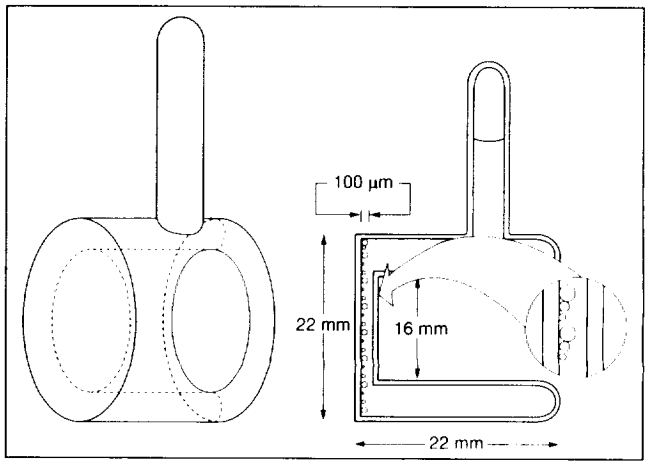

Fig. 5. Test cell schematic showing nucleated droplets on the front wall of the cell.

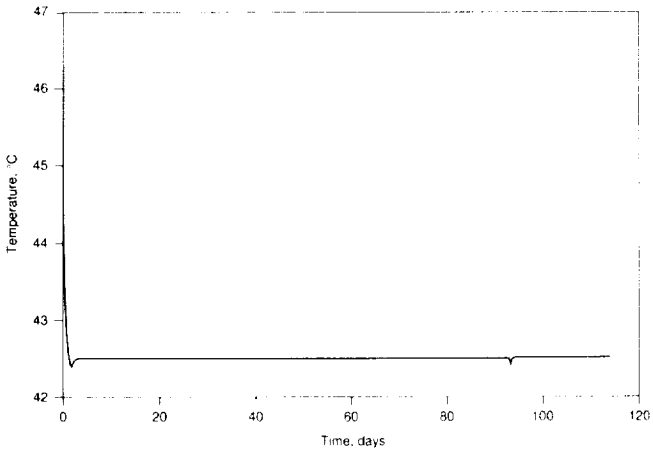

Fig. 6. Temperature history for the duration of the experiment.

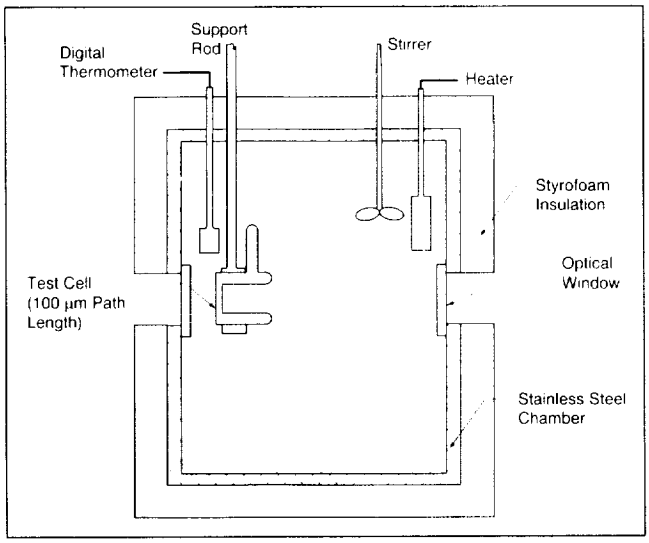

Fig. 7. Schematic of isothermal test chamber.

appropriate volume fraction and good thermal control. The temperature profile for the duration of the experiment is shown in Fig. 6.

Figure 7 is a schematic of the experimental apparatus. The test cell is positioned in a temperature-controlled water bath, an insulated stainless steel chamber with optical windows. A 0.2 μm filter element removed particles from the bath water that would interfere with holographic images. A thermistor in the bath was one leg of a ESI Model 250DE Wheatstone bridge and served as the feedback mechanism to provide control to a resistance heater in the bath. A Brookfield counter-rotating stirrer provided adequate stirring without entraining air in the water. Using this system, temperatures in the bath were controlled to 0.030°C over 94% of the experiment and 0.002°C for the first week of the 112-day observation. Performing the experiment near the isopycnic temperature minimized the effects of buoyancy.

Holographic Data

The time interval between holograms was initially 2 min. As the rate of change in droplet size distribution decreased, the time interval between holograms increased to two per day and finally to one per day. Each hologram is a record of the wavefront received by the film and contains all the optical information from the test cell for the instant in time when that hologram was made. When the hologram is reconstructed, the entire volume between the optical flats of the cell can be examined using various optical analysis tools which were not compatible with the test cell *in situ*. Details regarding the holographic construction and reconstruction systems can be found in Witherow[9] and Witherow and Facemire.[10] This holographic system gives a resolution of about 5 μm for the reconstructed image.

Reconstructed images from the holograms projected on the lens of a Dage MTI 70D video camera provided input for image analysis. The number of video fields required to span the diameter of the test cell in the reconstructed image and measurement of the test cell diameter determined the magnification factor for video-based droplet measurements. Using this magnification, the image of a single field comprised an area of 552 × 407 μm. Although the entire volume is available for study, the investigation examined a representative region of the test cell indicated in Fig. 1. One aim of this investigation, exploration of local interparticle interactive effects on the ripening processes, dictated use of contiguous rather than random fields. A 5 by 5 field section (25 fields), $5.617 \times 10^6\ \mu m^2$, represents a volume of 5.617×10^4 cc, approximately 5% of the observable volume located within the optical viewing area of the test cell. Virtually all droplets focus in the same plane, indicating that they are located in the same plane. Further, they do not move at all over the lengthy duration of the experiment, indicating attachment to the same wall of the cell. This is to be anticipated because during the quench, the front wall of the test cell experienced the cooler temperature first because of reduced cooling fluid circulation on the sheltered back wall (Fig. 5). The stagnant fluid in the sheltered portion of the test cell cooled more slowly than the front wall. Therefore, droplets nucleated on the cooler, front face of the test cell.

RESULTS AND DISCUSSION

Of the 152 holograms obtained during the experiment, the first 25 were taken as the cell cooled to the operating temperature, 42.5°C. The remaining holograms at this temperature, clearly show the ripening of the droplet phase over time. Figure 8 shows a series of photographs from reconstructed holograms. The data reported here reflect measurements taken from 14 of the 152 holograms, selected at intervals spanning the duration of the experiment. Table I lists the hologram number and recording time for each hologram studied. Recording time indicates time elapsed since initiation of the quench sequence.

Calculations using density data of compositions (majority phase, 93 mole% H_2O; minority phase, 48 mole% H_2O) taken from the phase diagram tie line at the experiment operating temperature indicate a

volume fraction of the succinonitrile rich droplet phase of approximately 2.75%. The emphasis of this study is the evolution of a droplet size distribution due to diffusional growth. Therefore, quantitative analysis of this long-term growth process could not begin until the volume fraction of the discrete phase became constant. Figure 9 shows the volume of the droplet phase in the viewing volume as a function of time. Calculation of total droplet volume assumes uniform shape for the droplets. This approximation is consistent with observations of wetting of succinonitrile-rich phase on quartz as shown in Fig. 4. Figure 9 indicates that the constant volume condition is attained by the second observation (1.2 days). Once constant volume is achieved, the average total volume of the droplet phase within the viewing volume did not exceed 1.4×10^{-5} cm^3, the maximum deviation from this value is 5%. This corresponds to a maximum volume fraction of 2.5%. This is, within the limits of experimental error, in good agreement with the volume fraction of 2.75%, calculated from the phase diagram.

Theoretical analysis of ripening processes generally considers the long-time asymptotic behavior. Figure 10 is a plot of the number of droplets within the field of view as a function of time. Linear regression performed on the observations indicates that in the later stages of the experiment, the slope of the curve achieved a value of –0.733, with a correlation coefficient of 0.994. The geometry of our experiment is represented by spherical caps located on a substrate interacting through two-dimensional diffusion fields, as indicated in Figure 5. Chaklaverty[4] developed expressions for growth of a discrete phase of spherical caps on a two-dimensional substrate due to surface diffusion. His analysis indicates that N scales as $t^{-3/4}$. Our experimental results for the rate of droplet decay are in good agreement with this value.

Figure 11 shows the change in average droplet radius as a function of time. During the reported period of observations, a 138% increase in average radius is realized. The analysis of Chakraverty[4] predicts that r scales as $t^{1/4}$ in the asymptotic limit. The plot of r vs time shown in Fig. 12 reveals that in the asymptotic limit (after ~2.5 weeks) the slope of the best fit line through these data is 0.247 with a correlation coefficient of 0.986. Again, our experimental data show agreement with the trends predicted by theory.

Statistically, self-similarity is a hallmark of the Ostwald ripening effect.[1,2,6] Theoretical analysis shows

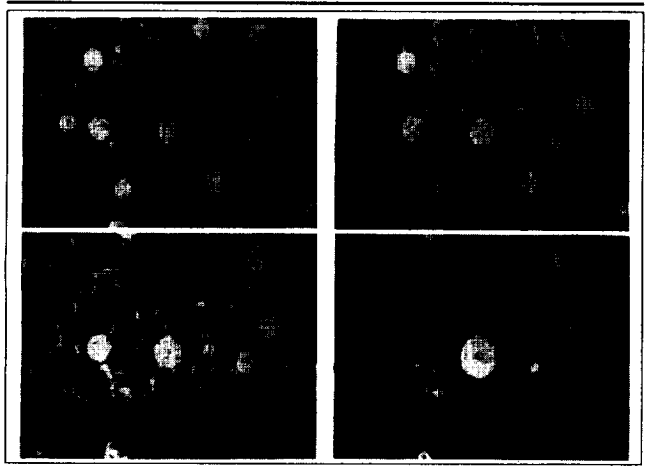

Fig. 8. Photographs from four holograms of the same field-of-view which show ripening effects over a period of several months.

Table I. Numbers and Recording Time for Studied Holograms

Hologram Number	Time, Seconds
20	1.6×10^4
30	1.06×10^5
40	5.4×10^5
50	1.07×10^6
61	1.5×10^6
70	2.0×10^6
80	2.5×10^6
90	3.1×10^6
100	3.7×10^6
110	4.5×10^6
120	5.7×10^6
130	7.2×10^6
140	8.1×10^6
152	9.8×10^6

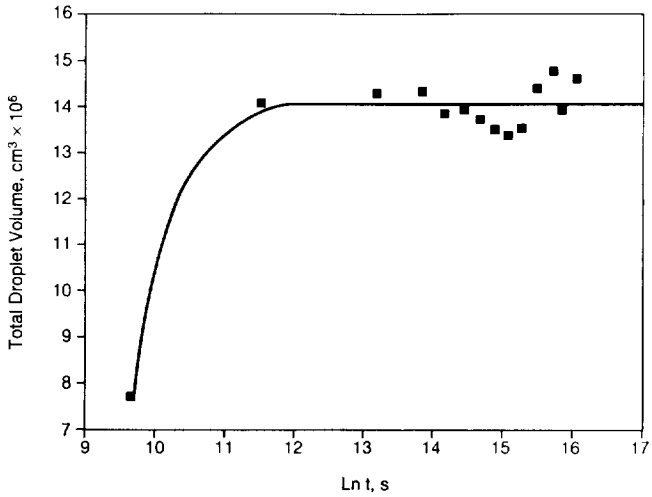

Fig. 9. Total droplet volume as a function of time.

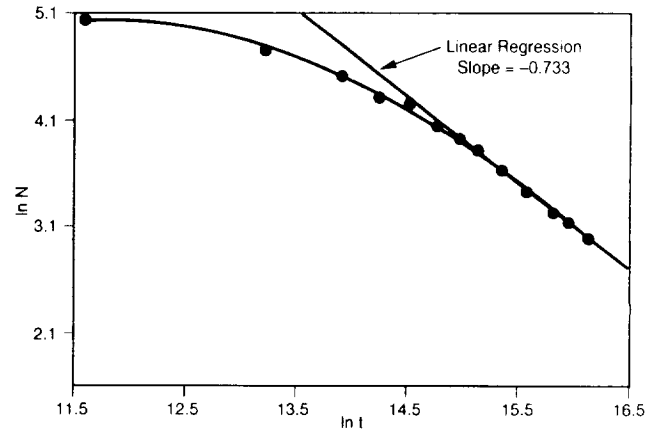

Fig. 10. Number of droplets in the selected area as a function of time.

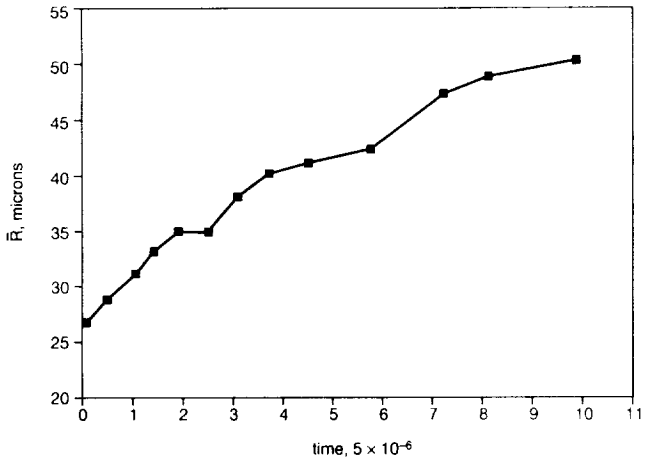

Fig. 11. Average radius as a function of time.

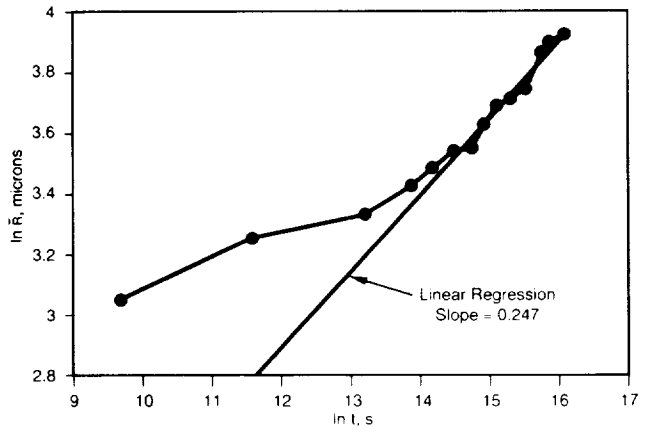

Fig. 12. Ln average radius as a function of Ln time.

that a scaled-time-independent droplet radius distribution function exists.[6,11] Morphological configurations during Ostwald ripening should remain statistically equivalent when examined under appropriately scaled magnifications. Figure 13 shows photographs taken directly from selected holograms during the ripening experiment. Photographs were taken to show a large portion of the test cell contents (approximately 50% of the area shown in hologram 151, or 1.08 cm^2). It is important to note that the droplets create interference fringes on these pictures. Droplets are the bright spots surrounded by the halo-like interference fringes. Additionally, bright spots occur inside the small droplets, which act as lenses. The magnification factors have been scaled with the average droplet radii. The photographs show very similar size distribution characteristics. Quantitative assessment of statistical self-similarity requires a great deal of additional data. Efforts to measure the size histories of additional droplets are presently under way.

Holography enables the study of local environment effects on the rate of droplet growth. Figure 14 shows the droplet size history of a centrally located portion of the viewing region in the vicinity of Field 19. Asterisks denote locations of droplets consumed due to the ripening process. Field 19 contained droplets 141–146. Figure 15 is a plot of the droplet diameters by hologram number. Note that the curve for droplet 145 intersects the curves for droplets 143 and 141. Classic ripening theory predicts that the larger droplets in a population should grow; the individual droplet trajectories should not cross. A careful examination of Fig. 14 reveals that droplet 145's spatial location favors diffusional interactions with droplet 171 in Field 23; droplet 145 shrinks and eventually disappears due to local effects.

Local effects also become evident in an examination of the critical radius. The critical radius at a given time in the experiment can be considered that droplet size at which there is no net flux of material to the droplet, where dR/dt = 0.00. Figure 16 shows plots of rate of change of droplet radii for selected holograms during the ripening stage of the experiment and the value of R_c predicted by theory. Theory suggests a single value for the critical radius given by

$$R_c(t) = \frac{9}{8}\bar{R}(t).$$

Examination of Fig. 16 reveals no observable rate of change in droplet radius for a range of values of droplet radii. The local environment of each specific droplet determines the critical radius within that environment. This range of values could be considered "microstructural fluctuations" and indicates the range of deviations from theoretical predictions. It is also evident that, within the resolution of the method, droplets of the same size appear to grow and shrink over the same time interval. This range of deviations may be a better predictor of the ultimate properties and function of the material in applications than the theoretical value of the "global critical radius."

CONCLUDING REMARKS

This study demonstrates limitations of mean field approaches which adequately predict scaling laws but not local droplet behavior during Ostwald ripening. Mean field theories incorporate use of a screening length (often suggested as $l_{sc} \approx 2$ droplet radii). Droplets spaced farther apart than that distance should grow or shrink only in response to differences between the concentration of the diffusing species at the surface of the droplet as defined by the Gibbs-Thompson equation and the mean field concentration. There is no direct interdroplet communication at distances which exceed l_{sc}. Therefore, where the interdroplet spacing exceeds ≈2 radii, all droplets larger than R_c should grow, all those smaller than R_c should shrink. Additionally, droplets of the same size should change size at the same rate. Data from this experiment indicates otherwise. The mean field approach is not sufficient to describe the behavior of individual droplets. Droplet interactions must occur in a more direct manner than suggested by the simple mean field approach.

In order to explore direct droplet interactions, the behavior of droplets with respect to size was examined. Surprisingly, the data includes observations in which droplets larger than their nearest neighbor

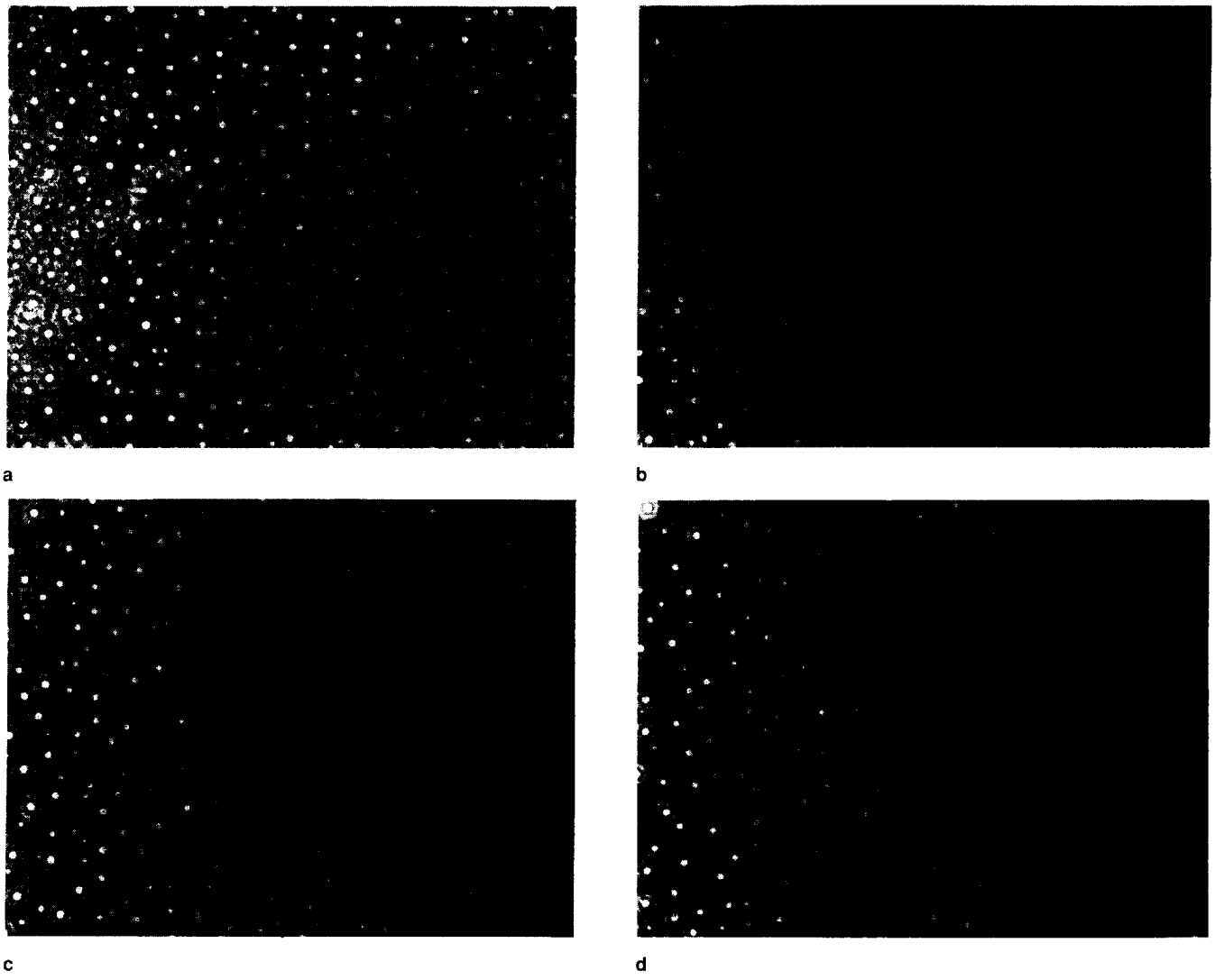

Fig. 13. Photographs of test cell at variable magnification for selected holograms: (a) HG 90, $t = 3.1 \times 10^6$ s; (b) HG 100, $t = 3.7 \times 10^6$ s; (c) HG 120, $t = 5.7 \times 10^6$ s; (d)HG 151, $t = 9.8 \times 10^6$ s.

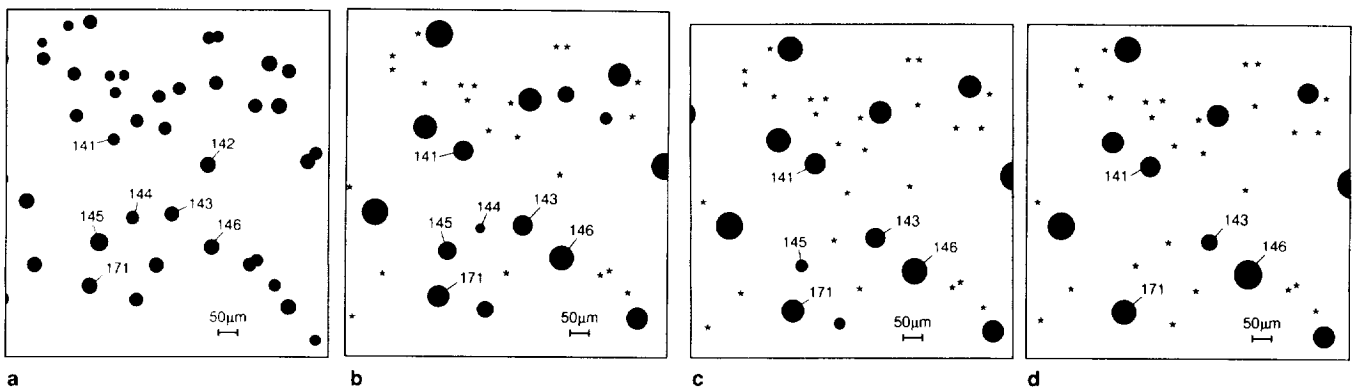

Fig. 14. Representation of droplets located near Field 19: (a) HG 20,$t = 1.6 \times 10^4$ s; (b) HG 80, $t = 2.5 \times 10^6$ s; (c) HG 90, $t = 3.1 \times 10^6$ s; (d) HG 100, $t = 3.7 \times 10^6$ s.

shrunk (and droplets smaller than their nearest neighbor grew). Clearly, these droplets were responding to the influence of droplets other than their nearest neighbor. The data suggests that the drop-size histories of individual droplets depends greatly on the details of the local environment. The simple approach of observing the interaction between a droplet and its nearest neighbor quickly becomes complicated when that nearest neighbor has another neighbor which is closer in another direction. The effects of the local

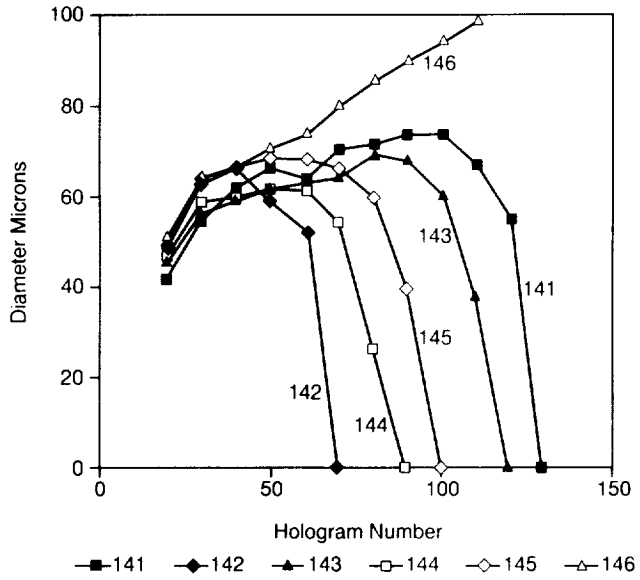

Fig. 15. Individual droplet lifetime trajectories.

environment on the behavior of a specific droplet are subtle. Understanding requires the application of modeling techniques which can account for the nature of diffusional interactions of the droplets in the ensemble. An additional complicating factor which is not addressed in the present studies is the possible effects of residual concentration nonuniformities as droplets become smaller than the resolution of the observation system. Droplets of less than approximately 2–3 μm are below these limits.

This study also exemplifies the benefits of holography. Using conventional microscopy, only one field-of-view would be accessible during a given instant in time. Holographic microscopy allows reconstruction of the test cell image and extraction of full details regarding the local environment of a given droplet. Future plans include the application of phase shifting interferometry to the holograms of the experiment in order to determine the concentration field in the test cell. Direct assessment of the concentration field should greatly enhance the understanding of diffusive growth processes.

Computer modeling provides an important bridge between theoretical predictions and experiments. Part II of this paper describes computer modeling studies which examine multiple droplet interactions to account for the observed local effects. The model includes droplet interaction parameters for the entire ensemble of droplets observed during this experiment. Predictions from the model are compared to experimental observations reported in this paper.

ACKNOWLEDGMENT

These studies were supported by NASA's Office of Space Science and Applications.

REFERENCES

1. I.M. Lifshitz and V.V. Slyozov, *J. Phys. and Chem. of Solids* 19, 35 (1961).
2. S.C. Wagner, *Z. Electrochemic* 65, 581 (1961).
3. O.M. Todes, *Zh. Fis. Khim. (Sov. J. Phys. Chem.)* 20, 629 (1946).
4. B.K.Chakraverty, *J. Phys. Chem. Solids* 28, 2401 (1967).
5. V.V. Slyozov, *Fis. Tverd. Tela* 9, 927 (1967).
6. M. Zinke-Allmany, L. C. Feldman and M. H. Grabow, *Surface Science Reports: A Review Journal* 16 (8), 377 (1992).
7. J.E. Smith, D.O. Frazier and W.F. Kaukler, *Scripta Met.* 18, 677 (1984).
8. D.O. Frazier and B.R. Facemire, *Thermochimica Acta.* 145, 301 (1989).
9. W.K. Witherow, *SPE* 18, 249 (1979).
10. W.K. Witherow and B.R. Facemire, *J. Colloid Interface Sci.* 104, 185 (1985).
11. P.W. Voorhees, *Ann. Rev. Mater. Sci.* 22, 197 (1992).

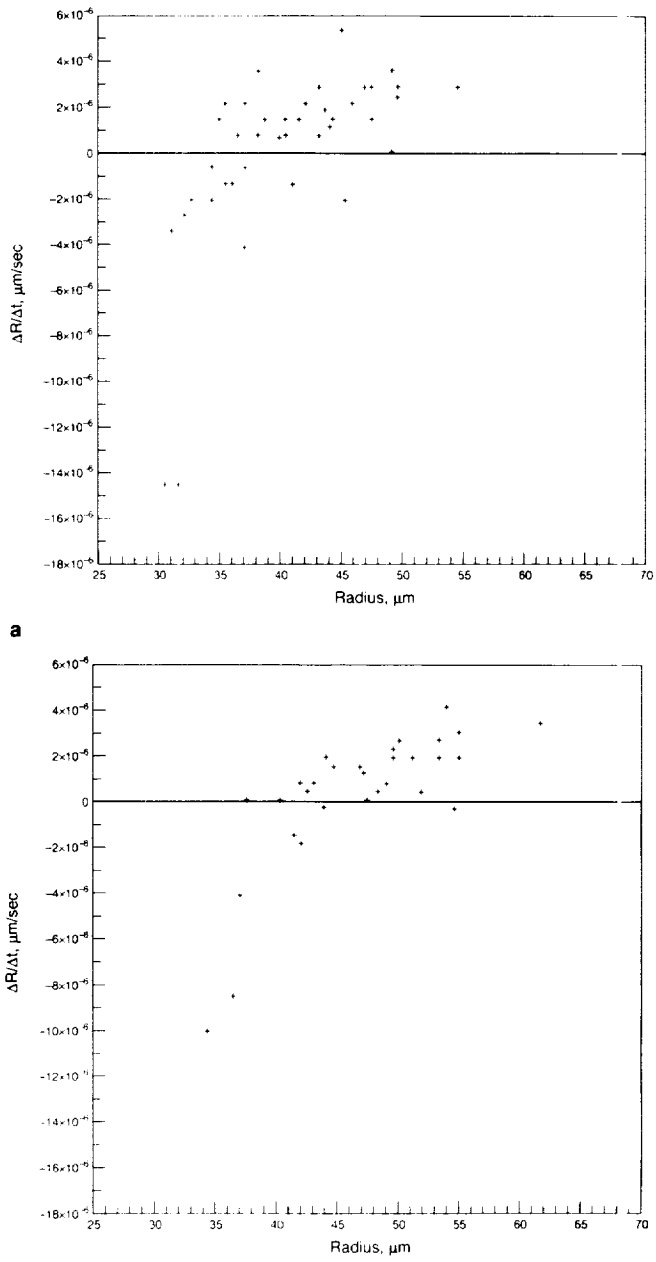

Fig. 16. Rate of change for droplet radii for holograms for selected intervals: (a) HG 100–HG 11; (b) HG 120–HG 130.